Distinct roles for two synaptotagmin isoforms in synchronous and asynchronous transmitter release at zebrafish neuromuscular junction

Hua Wen, Michael W. Linhoff, Matthew J. McGinley, Geng-Lin Li, Glen M. Corson, Gail Mandel[1], and Paul Brehm

Vollum Institute, Oregon Health and Sciences University, Portland, OR 97239

Contributed by Gail Mandel, June 16, 2010 (sent for review June 3, 2010)

An obligatory role for the calcium sensor synaptotagmins in stimulus-coupled release of neurotransmitter is well established, but a role for synaptotagmin isoform involvement in asynchronous release remains conjecture. We show, at the zebrafish neuromuscular synapse, that two separate synaptotagmins underlie these processes. Specifically, knockdown of synaptotagmin 2 (syt2) reduces synchronous release, whereas knockdown of synaptotagmin 7 (syt7) reduces the asynchronous component of release. The zebrafish neuromuscular junction is unique in having a very small quantal content and a high release probability under conditions of either low-frequency stimulation or high-frequency augmentation. Through these features, we further determined that during the height of shared synchronous and asynchronous transmission these two modes compete for the same release sites.

active zone | exocytosis | synapse | acetylcholine receptor

A hallmark of synaptic transmission is the synchrony between the neuronal action potential and the evoked release of transmitter. However, an asynchronous release mode, first described at the nerve muscle junction (1, 2), also participates in neurotransmission at certain synapses (3–5). Although asynchronous release usually contributes less than 10% of the overall synaptic charge at low stimulus frequencies, it often plays a prominent role at higher frequencies (3, 6), prolonging both inhibitory (7) and excitatory (8, 9) postsynaptic responses through sustained release. Indeed, inhibitory deep cerebellar neurons, which are tuned for high-frequency signaling, rely exclusively on asynchronous synaptic transmission at contacts with inferior olive neurons (10). The mechanisms underlying synchronous and asynchronous release appear to be distinct but share a requirement for calcium (6, 11). It is generally thought that local transient calcium signals govern synchronous release, whereas elevated residual calcium levels associated with high-frequency stimulation lead to asynchronous release (12, 13).

A vesicular calcium sensor, synaptotagmin, couples synchronous release to presynaptic calcium entry in both mammals (14) and flies (15, 16). In hippocampus, the responsible isoform is syt1 (14, 17), whereas at neuromuscular synapses (18) and calyx of Held (11, 19), it is syt2. The mechanisms underlying asynchronous release are not known. Our findings from zebrafish neuromuscular junction provide identification of a synaptotagmin isoform as a signaling component in asynchronous release.

Results

Paired Recordings Reveal a Small Quantal Content with Release Probability Near "1." Paired whole-cell recordings between the caudal primary motor neuron (CaP) and ventral target skeletal muscle were performed on 72- to 96-h-postfertilization (hpf) zebrafish as previously described (20). The motor neuron was current clamped to −80 mV and stepped positive for 2 ms to elicit an action potential. The fast-type skeletal muscle was voltage clamped to −50 mV to inactivate sodium channels. The amplitude for spontaneous unitary events (miniature endplate currents, mEPCs) was normally distributed with a mean quantal size of 536 ± 205 pA (n = 9 cells; >100 events per cell). At a stimulus frequency of 0.2 Hz, the peak amplitudes of successive evoked endplate currents (EPCs) showed little variability, as reflected in the small coefficient of variation (0.1 ± 0.02, n = 11). In 2.1 mM calcium, the EPCs recorded at 0.2 Hz were, on average, 10-fold larger than the average mEPC. The quantal content for each recording, estimated by dividing the average EPC amplitude obtained at 0.2 Hz by the mean mEPC amplitude, corresponded to 9.6 ± 2.9 (n = 22). Increasing the extracellular calcium concentration from 2.1 to 10 mM did not alter quantal content, indicating that the release probability had reached a maximum at 2.1 mM.

The low variance in EPC amplitude and failure to increase amplitude with elevated extracellular calcium both pointed to a release probability near 1 at physiological calcium levels. This idea was further supported by two quantitative approaches. First, the variance in EPC amplitudes at 0.2 Hz was used to predict the variance of mEPCs for each recording, by dividing the EPC variance by the quantal content. The estimated mEPC standard deviation (165 ± 34 pA; n = 11) could be fully accounted for by the measured mEPC standard deviation (205 ± 40 pA; n = 9). Second, a multinomial model of release was used to estimate the release probability and number of available release sites for each recording from the variability measured for mEPCs and for EPCs evoked at 0.2 Hz (*Materials and Methods* and ref. 21). The predicted release probability ranged from 0.86 to 0.97 (0.91 ± 0.03; n = 11) and the predicted number of release sites was 10.6 ± 3.4.

Quantifying Synchronous and Asynchronous Release Components. To initiate synchronous and asynchronous release, 100-Hz stimulus trains were delivered for 10 s, resulting in near-complete depression of EPCs (Fig. 1*A*). During the first second of stimulation, the endplate currents were almost entirely phase locked to the repolarization phase of the presynaptic action potential (Fig. 1*A1*) after which a transition to mixed synchronous and asynchronous release occurred (Fig. 1*A2*). Then, the transmission transitioned into highly non-phase-locked, asynchronous release (Fig. 1*A3*). To quantify release, we measured the total charge by integrating the synaptic current for each 10-ms interval (Fig. 1*B* black symbols). As an alternative approach, we also summed synaptic current amplitudes for each interval (Fig. 1*B* red symbols). Because the kinetics of the synchronous and asynchronous events appeared similar, these two methods of quantification

Author contributions: H.W., G.M., and P.B. designed research; H.W., M.W.L., and G.M.C. performed research; H.W., M.J.M., and G.L. analyzed data; and G.M. and P.B. wrote the paper.

The authors declare no conflict of interest.

Freely available online through the PNAS open access option.

Data deposition: The sequence reported in this paper has been deposited in the GenBank database (accession no. GU591155).

[1]To whom correspondence should be addressed. E-mail: mandelg@ohsu.edu.

This article contains supporting information online at www.pnas.org/lookup/suppl/doi:10.1073/pnas.1008598107/-/DCSupplemental.

www.pnas.org/cgi/doi/10.1073/pnas.1008598107

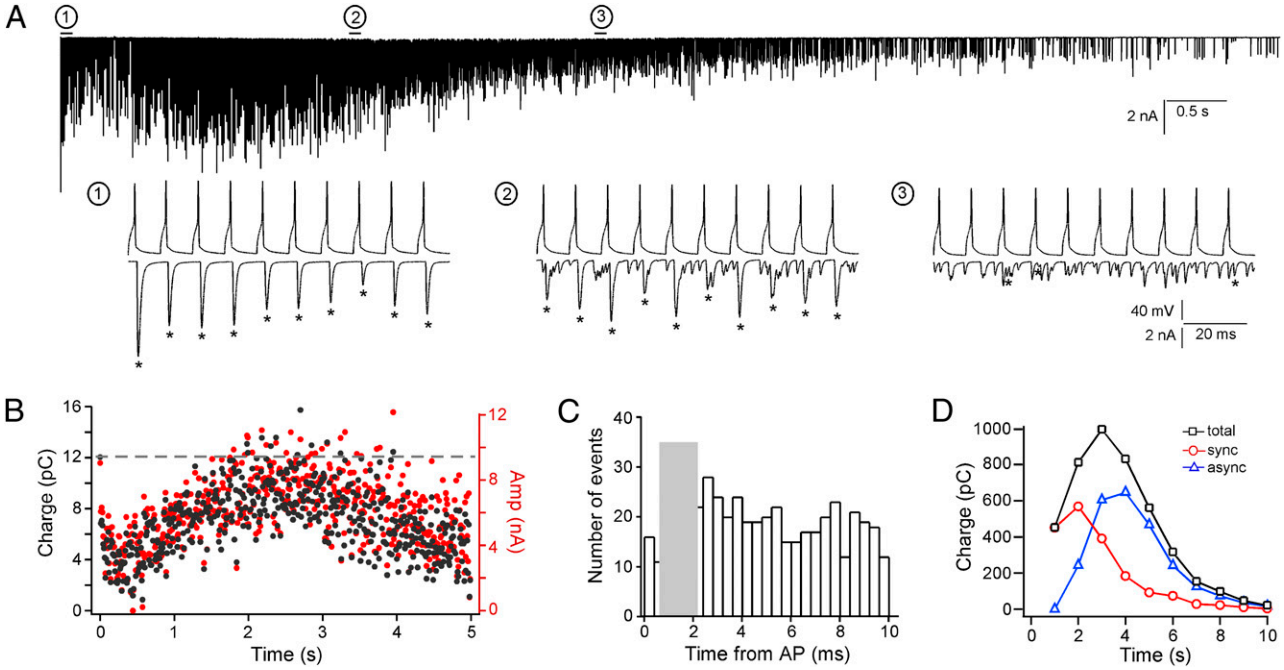

Fig. 1. Quantification of synchronous and asynchronous components of release. (*A*) A 10-s recording of EPCs in response to 100 Hz stimulation. Regions are expanded on a fast time scale along with the motor neuron action potentials corresponding to purely synchronous (*A1*), to shared synchronous and asynchronous (*A2*), and to largely asynchronous release (*A3*). Asterisks indicate synchronous events. (*B*) Scatterplot of total integrated release (black circles) and summed amplitudes (red circles) for each 10-ms interval occurring during the first 5 s of a representative paired recording as shown in *A*. The horizontal line represents the maximal predicted release corresponding to amplitude of the first EPC of the train, before the onset of depression. (*C*) A frequency histogram of time intervals between each asynchronous event and the peak of the action potential during the 3- to 4-s window of the stimulation. The gray bar indicates the 1.5-ms window used to score events as synchronous. (*D*) The contributions by synchronous (red circles) and asynchronous (blue triangles) release for each second interval were obtained by integrating the charge associated with each process during sequential 10-ms intervals shown in *B*. The total charge contributed by the sum of the two modes is shown by the black squares.

would be expected to produce the same relationships; this was indeed the case (Fig. 1*B*). To further quantify the contributions by synchronous and asynchronous release during each 10-ms interstimulus interval, the two components were separated on the basis of timing with respect to the peak of the presynaptic action potential. Release was considered synchronous when the peak synaptic current occurred within a 1.5-ms window that started 0.6 ms after the peak of the motorneuron action potential (Fig. 1*C*). The initial 0.6-ms period corresponds to the synaptic delay at this synapse (20). The additional 1.5 ms represents the time required for rise and decay of synaptic current. Any synaptic responses that occurred before or after the 1.5-ms time window were considered asynchronous. The non-phase-locked, asynchronous, events occurred throughout the 8.5-ms asynchronous period (Fig. 1*C*). Consecutive 10-ms intervals were binned into 1-s intervals to chart the time course for each component (Fig. 1*D*). These plots consistently showed a trend from principally synchronous to principally asynchronous transmission over the 10-s period of stimulation, with asynchronous release accounting for 53.7 ± 7.9% (n = 11) of total release. This is an underestimate, due to the likelihood of asynchronous release occurring during the 1.5-ms window that was scored as synchronous.

At 100 Hz, the total charge associated with each 10-ms interval showed an initial depression after the first EPC (Fig. 1*B*). The first EPC corresponded to a probability of release near unity and will be referred to as maximal predicted release (indicated by a reference line in Fig. 1*B*). After sustained stimulation for 2 s, the EPCs exhibited augmentation wherein the total amount of release during some 10-ms intervals returned near the maximal predicted level. This would be expected to occur if all of the release zones were able to reload during 10 ms, a rate that was independently confirmed by recovery curves performed at different stimulus frequencies. Inspection of those 10-ms intervals, where the summed integrated release was >80% of maximal predicted release suggested a reciprocity between asynchronous and synchronous release (Fig. 2*A*). The relationship between the amount of synchronous and asynchronous charge during these individual 10-ms intervals was well fit by a line with a slope near −1 (Fig. 2*B*). For 10 additional recordings, the slopes ranged from −0.85 to −1.10 with an overall mean value of −0.99 ± 0.08 and were independent of the total amount of releasable transmitter (Fig. 2*C*). The near-unity slope indicated that the total release per interval was constant, and equal to the predepression level, during the time of maximal sharing between synchronous and asynchronous release. Given that the release probability is near 1, these data support the idea that the two modes are competing for the same release machinery.

Role of Synaptotagmin 2 in Synchronous Release. Syt2 was tested because of its role in synchronous release at mammalian neuromuscular junctions (18). Zebrafish syt2 was identified on the basis of its amino acid identity to rat syt2 protein (72%). Translation of syt2 mRNA was blocked by injection of an antisense morpholino for the translational start site. An effective knockdown of syt2 protein was shown by immunohistochemical labeling with the syt2-specific antibody znp1 (ref 22; n = 15 fish; Fig. 3*C*). The reduction in syt2 protein was not associated with alterations in labeling for the synaptic vesicles and postsynaptic receptor clusters (Fig. 3*C*). The syt2 morpholino fish exhibited an increase of over 20-fold in the frequency of spontaneously occurring mEPCs (Fig. 3*D*). Increased frequency of spontaneous currents have also been reported for syt1 and syt2 knockout animals (15, 18, 23). Recordings from syt2 morpholino fish revealed a marked reduction in, but not complete elimination of

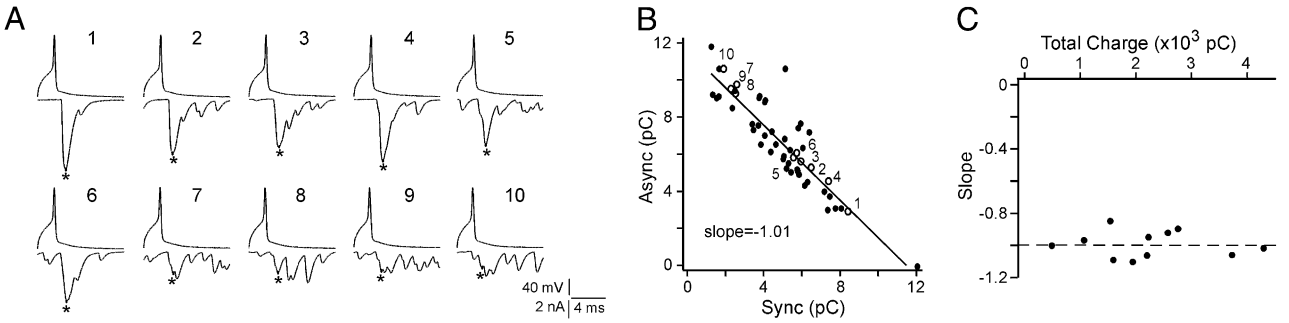

Fig. 2. Synchronous and asynchronous release competes for the same release machinery. (*A*) Recordings of the action potential and associated postsynaptic response for sample 10-ms intervals when sharing between synchronous and asynchronous was maximal. The synchronous component scored on the basis of the 1.5-ms window is indicated for each interval by an asterisk. (*B*) Intervals with total release corresponding to >80% of the maximal response (shown in Fig. 1*B* as dashed line) were used to compare the contributions by synchronous and asynchronous release during each 10-ms interval. The open symbols are the values for each of the numbered individual intervals shown in *A* and closed symbols represent the values for the intervals not shown in *A*. The distribution was best fit by linear regression to a line with a correlation coefficient of 0.81. (*C*) The slope values for each of 11 cell pairs are plotted against the total charge associated with each 10-s recording. The dashed line indicates a slope of −1. The average correlation coefficient of the linear fits (as shown in *B*) of the 11 pairs was 0.82 ± 0.05.

synchronous release (Fig. 3*A*). This was best reflected in the frequent failures observed during the initial second of stimulation (Fig. 3*A1*). The contribution of the release during the first second to the total release measured during 10 s stimulation was significantly less in syt2 morpholino compared with wild-type fish (5.5 ± 2.8% for syt2 morpholino, 12.0 ± 2.6% for wild-type fish; Fig. 6*C*). Because the first second represented a time where release was almost completely synchronized in wild type (95.4 ± 4.4%, $n = 11$), this reduction indicated that syt2 morpholino specifically affected synchronous release. The timed onset for asynchronous release appeared normal, but the relative contribution was greater than in wild-type fish (compare Figs. 1*D* and 3*B*). The overall release was not significantly different for syt2 morpholino and wild-type fish (Fig. 6 *A* and *B*). Due to the large variability in total release between recordings, we measured the fractional contributions of synchronous and asynchronous modes. During the overall 10 s of stimulation, the fractional contribution by synchronous release was significantly reduced from 46.3 ± 7.9% to 23.0 ± 7.6% ($n = 6$ fish; Fig. 6*D*). The fractional synchronous release during the height of release (the 3- to 4-s window) was not significantly different between syt2 morpholino and wild-type fish (Fig. 6*E*), likely resulting from greatly increased levels of asynchronous release at this time period of the stimulation.

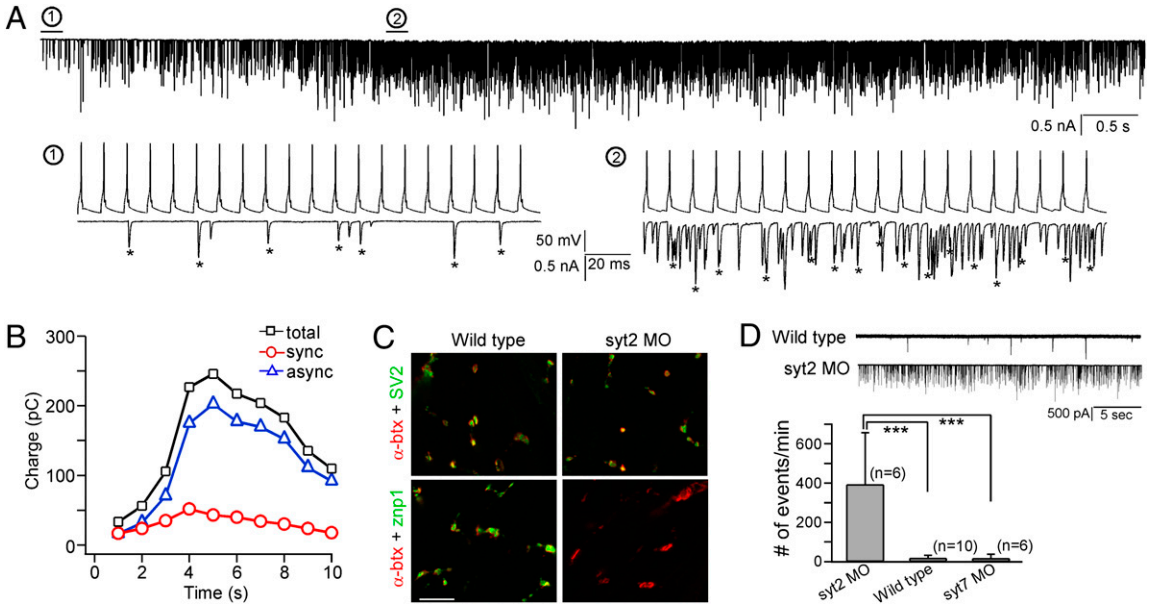

Fig. 3. Effects of syt2 knockdown on release. (*A*) The 10-s train of EPCs in response to 100-Hz stimulation for a syt2 morpholino fish. Two regions are expanded on a fast time scale corresponding to times when, in wild-type fish, release is either largely synchronous (*A1*) or asynchronous (*A2*). Asterisks indicate EPCs considered to be synchronous. The increased frequency of synchronous events in *A2* is likely due to the heightened probability that an asynchronous event will fall within the window defined for synchronous detection. (*B*) Comparison of the contributions of asynchronous (blue triangles) versus synchronous (red circles) to total release (black squares) over the time course of 10 s of stimulation. (*C*) SV2 presynaptic label (green) and postsynaptic α-bungarotoxin (α-btx) label (red) in wild type (*Upper Left*) and syt2 morpholino (*Upper Right*) fish. Znp-1 antibody labeled syt2 protein (green) colocalizes with α-btx (red) label in wild-type fish (*Lower Left*) but is absent in syt2 morpholino fish (*Lower Right*). (Scale bar, 10 μm.) (*D*) Example traces of spontaneous synaptic currents from wild type (*Top*) and syt2 morpholino (*Bottom*) fish. A bar graph of spontaneous event frequency for wild-type fish (392 ± 263; $n = 6$ recordings), syt2 morpholino fish (18 ± 14; $n = 10$ recordings), and syt7 morpholino fish (17 ± 21; $n = 6$ recordings). ***$P < 0.001$.

Role of Synaptotagmin 7 in Asynchronous Release. Syt 7 was tested for involvement in synaptic transmission because it had been proposed to mediate asynchronous release (24). The zebrafish syt7 gene was identified by homology search of the zebrafish genome using mammalian syt7 amino acid sequence. Both human and rat syt7 genes are composed of 14 coding exons, with exons 4–8 subject to extensive alternative splicing, thus producing a large number of transcripts (25, 26). Our database search found that sequences highly homologous to 12 out of 14 mammalian exons are present in the zebrafish genome, occupying a ~286-kb region on linkage group 7 (Fig. 4*A*). These include the N-terminal exons 1–3, C2-domain exons 9–14, and 3 out of 5 alternatively spliced exons (exons 4, 7, and 8). Overall, the zebrafish syt7 sequence is 70% identical to rat syt7 on the amino acid level (Fig. 4*A*), higher than for any other rat synaptotagmin isoforms and only 31% identical to zebrafish syt2. RT-PCR analysis on zebrafish larva revealed two syt7 amplicons, which upon sequencing were determined to represent splice variants. The major transcript contained exons 4 and 8 of the variable region in addition to the flanking constant exons (Fig. 4*B* lane 2). This splice pattern differs from all previously reported splice variants of mammalian syt7 genes (25, 26). The minor transcript contained exon 4, but lacked exon 8.

Several morpholinos were tested to identify candidates for disrupting syt7 mRNA splicing. RT-PCR analysis revealed one morpholino with a target sequence located near the 5′ end of exon 8 that strongly affected the splicing pattern (Fig. 4*B*). Sequence analysis of the RT-PCR products from syt7 morpholino-injected fish showed an increase in the transcript lacking exon 8, corresponding to the minor product in wild type, and a marked reduction of transcripts containing exon 8. Specifically, real-time RT-PCR experiments with primers designed to amplify exon 8 showed that morpholino-injected fish expressed the major transcript at only 8.8 ± 6.6% of the wild-type level (n = 4). To authenticate knockdown of syt7 protein by the morpholino, we generated a mouse polyclonal antibody. The specificity of the syt7 antibody was confirmed by in vivo ectopic expression of a syt7–mCherry fusion protein in skeletal muscle (Fig. S1). Using syt7 antibody, wild-type fish showed a fluorescent signal that colocalized with α-bungarotoxin, indicating that syt7 is synaptically located (Fig. 4*C*). In contrast, syt7 labeling was absent at the α-bungarotoxin puncta in the morpholino fish (n = 10 fish, Fig. 4*C*). Syt2 antibody labeling appeared normal in the syt7 morpholino fish (Fig. S2).

Recordings from syt7 morpholino fish revealed a striking specific reduction in asynchronous release, leaving the synchronous component intact (Figs. 5*A* and 6*A*). This was best reflected in the 3- to 4-s time window wherein asynchronous release contributes over 70% of release in wild type (compare Figs. 1*D* and 5*B*). During this time window, the contributions by synchronous release were 76.1 ± 12.7% for syt7 morpholino fish versus 27.5 ± 8.5% for wild type (Fig. 6*E*). The fractional release during the first second of recording is not significantly different for wild-type and syt7 morpholino fish (Fig. 6*C*), indicating that asynchronous release is specifically targeted by the morpholino. During the 10-s period the release components shifted to principally synchronous release (Fig. 6*D*; 71.2 ± 9.3% for 11 syt7 morpholino fish and 46.3 ± 7.9% for 11 wild-type fish). The magnitude of the individual components differed for syt2, syt7, and wild-type fish but the mean time required to achieve peak release was similar between the morpholino fish (Fig. S3). Unlike syt2, syt7 knockdown was not associated with significant changes in the frequency of spontaneous synaptic currents compared with wild type (Fig. 3*D*). In addition, there was no significant difference in total release between syt7 morpholino and wild-type fish, further pointing to a competition between the two modes for release (Fig. 6*B*).

Discussion

Zebrafish neuromuscular junction provides a unique opportunity to explore the basis of asynchronous synaptic transmission. First, the ability to use whole-cell voltage clamp for muscle recordings enabled full resolution of the unitary quantal events (20). Second, the fast decay kinetics and large quantal size facilitated the separation of individual synaptic events during high-frequency stimulation. Finally, a low quantal content and near unity probability of release provided a read out of individual release sites and their association with each mode of release.

We find that the total amount of available release was statistically indistinguishable for predominantly synchronous or asynchronous modes of release. This supports the assertion that they compete for the same populations of vesicles (4, 9, 11, 17) and argues against different vesicle types with different sensors (27). The issue as to whether synchronous and asynchronous modes act through shared or distinct release sites has been difficult to address, due primarily to the large numbers of release sites at most synapses studied. We took advantage of the augmentation in release probability that occurs in response to high-frequency stimulation, a phenomenon observed at a variety of

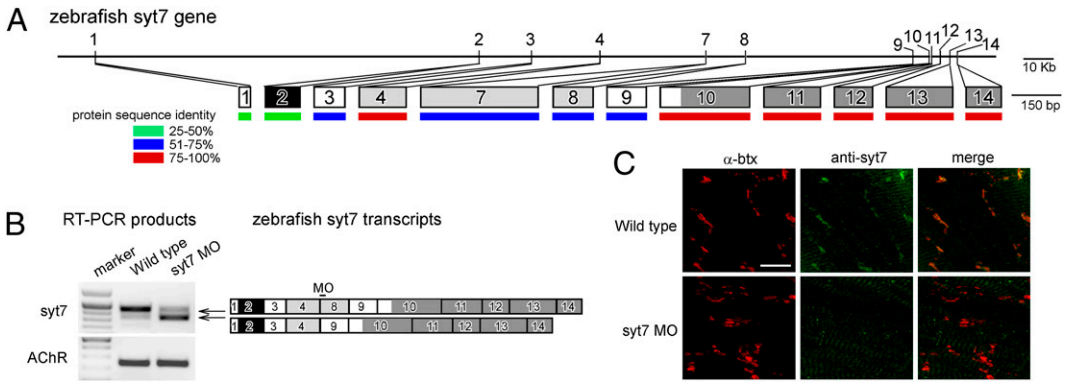

Fig. 4. Zebrafish syt7 gene and transcripts. (*A*) The location of exons on the gene (*Upper*) and transcript (*Lower*) are shown for zebrafish syt7. Exons are numbered on the basis of the mammalian gene (25, 26). The relative sizes of individual exons are indicated, along with the percentage identity to rat syt7 on the amino acid level (color indicators). The domains, predicted on the basis of homology to the mammalian gene are: transmembrane (black), calcium-binding C2 domains (dark gray), and alternatively spliced (light gray) regions. (*B*) RT-PCR analysis on wild-type and syt7 morpholino fish. The exon structures of the RT-PCR products and morpholino position are shown schematically. As a control the α-subunit of muscle acetycholine receptors was amplified from the same sample. (*C*) Syt7 antibody label (green) colocalizes with α-btx labeling (red) in wild type (*Upper*) but is absent at α-btx-labeled sites in syt7 morpholino fish (*Lower*). (Scale bar, 10 μm.)

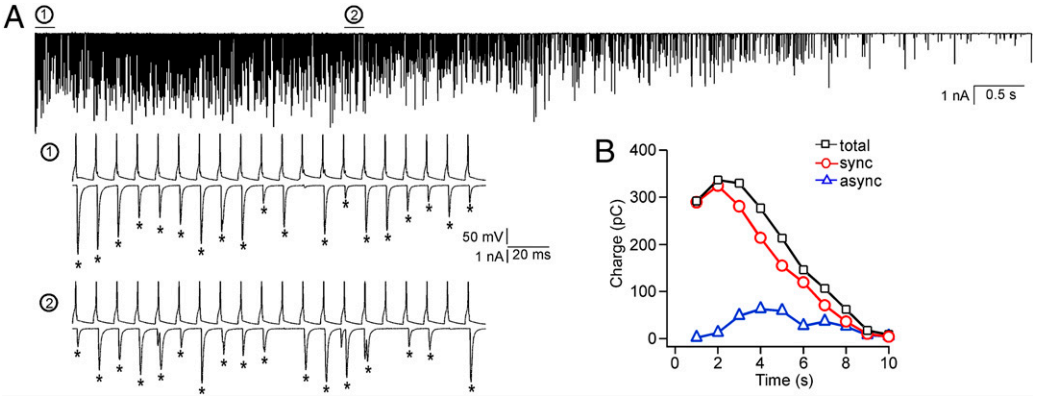

Fig. 5. Effects of syt7 knockdown on release. (*A*) A 10-s recording of EPCs in response to 100-Hz stimulation for a syt7 morpholino fish. Two regions are expanded on a fast time scale corresponding to times where, in wild-type fish, release is either largely synchronous (*A1*) or asynchronous (*A2*). (*B*) Comparison of the contributions of asynchronous (blue triangles) versus synchronous (red circles) to total release (black squares) over the time course of 10-s stimulation.

synapses (28–31). Our findings indicate that at the height of shared synchronous and asynchronous modalities, the summed total release during each 10-ms interval corresponded to the release associated with pure synchronous responses measured at low frequency stimulation, where the probability of release is near unity. This maximal level of release was maintained, despite the relative contributions by synchronous and asynchronous release during the 10-ms interval. This was reflected in the reciprocal relationships between synchronous and asynchronous release obtained for all of the recordings. We conclude that the two modes of release share the same set of release sites at zebrafish neuromuscular junction.

That a synaptotagmin calcium sensor underlies synchronous transmitter release is well accepted. At some neuronal synapses it is mediated by syt1 (14) but at the neuromuscular junction of mammals (18) and the calyx of Held (11, 19) it is mediated by syt2. We show that syt2 is also responsible for synchronous transmission at zebrafish neuromuscular junction. The observation that asynchronous release occurs in response to global elevations in internal calcium concentration helped fuel the idea that the asynchronous calcium sensor would have different calcium-binding features, such as those associated with syt7 (32–35). To date, the calcium sensor underlying asynchronous transmission has not been established for any synapses, but syt7 has been shown to mediate release of dense core vesicles from endocrine tissue and PC12 secretory cells (25, 32, 36–38). Our findings support the idea that syt7 is involved in asynchronous release at the zebrafish neuromuscular junction. In opposition to syt7 serving as the asynchronous sensor, recordings from cortical neurons derived from syt7 knockout mice failed to reveal effects on asynchronous release (39). This raises the possibility that effects of syt7 knockdown in zebrafish are indirect, perhaps through altered calcium handling. However, our finding that asynchronous release is significantly reduced in syt7 knockdown versus syt2 knockdown with no accompanying change in time course argues against this idea. It seems more likely that calcium sensors other than syt7 may be involved at different synapses like those between cortical neurons. Recently, synaptotagmin-like doc2b was shown to mediate spontaneous transmitter release with no role in either synchronous or asynchronous synaptic transmission (40). Together with our results from zebrafish neuromuscular junction, the number now stands at three different calcium-sensing molecules shown to be involved in functional distinctions among spontaneous, synchronous and asynchronous release modes. It remains important to determine whether syt7 plays a role at other synapses, particularly where asynchronous release represents the predominant form of synaptic transmission.

Materials and Methods

Data Analysis and Statistics. Patch clamp recordings from the CaP neuron and fast skeletal muscle were performed as described previously (20). Synaptic

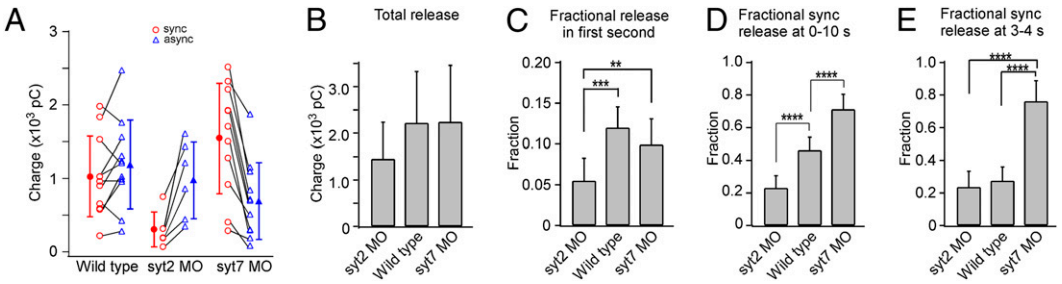

Fig. 6. Quantitative overall comparisons of the effects of syt2 and syt7 morpholinos on synchronous and asynchronous release components. (*A*) Scatterplot of the charge associated with synchronous (red circles) and asynchronous (blue triangles) for the individual recordings from wild type, syt2 morpholino, and syt7 morpholino fish. The black lines connect the charges associated with asynchronous and synchronous contributions in each individual recording. (*B*) The total release over 10 s for syt2 morpholino (n = 6 cells), syt7 morpholino (n = 11 cells), and wild-type (n = 11 cells) fish were comparable (F = 1.36; P = 0.27). (*C*) Comparison of the contribution of summed release during the initial second of stimulation, to the total summed release measured over the entire 10-s period (F = 9.96; $P < 0.0001$). For pairwise comparisons, $^{**}P < 0.02$; $^{***}P < 0.0005$. (*D*) Comparison of the fraction of release that occurred synchronously over the 10 s of stimulation (F = 66.4; $P < 1 \times 10^{-11}$). (*E*) Comparison of the fraction of the release that occurred synchronously during the 3- to 4-s window of stimulation (F = 74.9; $P < 5 \times 10^{-11}$). The values have not been corrected for contamination by asynchronous or spontaneous events. This will overestimate the contribution by synchronous release, particularly for syt2 knockdown where asynchronous and spontaneous release are elevated. For pairwise comparisons in *D* and *E*, $^{****}P < 1 \times 10^{-10}$.

currents were analyzed offline using MiniAnalysis (Synaptosoft), Clampfit (Molecular Devices), or IGOR Pro (WaveMetrics). The release probability and number of available release sites were estimated from the amplitude variability in mEPCs and EPCs evoked at 0.2 Hz. In one model, assuming between site variability, we assumed multinomial release statistics and uniform release probability across sites. The number of release sites, for each cell, was calculated as: $N = \frac{Q}{q - \frac{Q \cdot CV_q^2}{1 + CV_q^2}}$, where N = number of release sites; Q = mean EPC amplitude; q = mean mEPC amplitude; CV_Q = coefficient of variation of EPC amplitude; and CV_q = coefficient of variation of mEPC amplitude. The predicted release probability for each cell was calculated as the quantal content divided by the predicted number of release sites (21). The second model consisted of a simple comparison between the mEPC and EPC variance, assuming all variability occurs within a site.

Statistical significance was assessed using ANOVA, and group F value and P value are reported. Pairwise comparisons were made using Tukey's post hoc test, and P values are reported. Data were presented as mean ± SD.

RT-PCR Analysis and Morpholino Injection. The zebrafish syt2 and syt7 genes were identified on the basis of protein sequence similarity to the mammalian syt2 and syt7 using the NCBI Blast program (www.ncbi.nlm.nih.gov/BLAST). The GenBank accession number for zebrafish syt2 is XM_683000 and for syt7 is GU591155. Total RNA was isolated from wild-type fish between 72 and 96 hpf. First-strand cDNA synthesis was performed with SuperScript III reverse transcriptase (Invitrogen). RT-PCR products were either sequenced directly or cloned into pCR4-TOPO vector (Invitrogen) and sequenced.

Morpholino oligonucleotides were synthesized by Gene Tools. The sequence for syt2 morpholino is 5′ AGGTTCCACTTCATGATCTCTGGCT 3′ and for syt7, is 5′ CGATGGCGAGAGACAAAACCACCAT 3′. A total of 4 ng of syt2 morpholino and 1 ng of syt7 morpholino were injected into wild-type eggs at the single-cell stage.

Immunohistochemistry. SV2 and znp1 (syt2 specific) antibodies were acquired from Developmental Studies Hybridoma Bank. A mouse polyclonal antibody to zebrafish syt7 was generated by immunizing BALB/c female mice four times with a CMV–synaptotagmin7 plasmid at 2- to 3-wk intervals. The animals received 200 μg of plasmid in the tibialis anterior muscle in 50 μL of PBS, followed immediately by square wave electroporation (CUY21 EDIT, Nepa Gene) (41).

ACKNOWLEDGMENTS. We thank Dan Cawley (Oregon Health Sciences University Vaccine and Gene Therapy Institute, Portland, OR) for generating the syt7 antibody. We thank Huilan Yao for help with real time RT-PCR experiments. This project was supported by a National Institutes of Health Grant to P.B. (NS-18205) and a National Research Service Award to M.J.M. (NS-058196). Gail Mandel is an investigator of the Howard Hughes Medical Institute.

1. Feng TP (1941) The changes in the endplate potential during and after prolonged stimulation. *Chin J Physiol* 13:29.
2. Eccles JC, Katz B, Kuffler SW (1941) Nature of the endplate potentials in curarized muscle. *J Neurophysiol* 4:6.
3. Lu T, Trussell LO (2000) Inhibitory transmission mediated by asynchronous transmitter release. *Neuron* 26:683–694.
4. Hagler DJ, Jr, Goda Y (2001) Properties of synchronous and asynchronous release during pulse train depression in cultured hippocampal neurons. *J Neurophysiol* 85: 2324–2334.
5. Goda Y, Stevens CF (1994) Two components of transmitter release at a central synapse. *Proc Natl Acad Sci USA* 91:12942–12946.
6. Atluri PP, Regehr WG (1998) Delayed release of neurotransmitter from cerebellar granule cells. *J Neurosci* 18:8214–8227.
7. Hefft S, Jonas P (2005) Asynchronous GABA release generates long-lasting inhibition at a hippocampal interneuron-principal neuron synapse. *Nat Neurosci* 8:1319–1328.
8. Iremonger KJ, Bains JS (2007) Integration of asynchronously released quanta prolongs the postsynaptic spike window. *J Neurosci* 27:6684–6691.
9. Otsu Y, et al. (2004) Competition between phasic and asynchronous release for recovered synaptic vesicles at developing hippocampal autaptic synapses. *J Neurosci* 24:420–433.
10. Best AR, Regehr WG (2009) Inhibitory regulation of electrically coupled neurons in the inferior olive is mediated by asynchronous release of GABA. *Neuron* 62:555–565.
11. Sun J, et al. (2007) A dual-Ca2+-sensor model for neurotransmitter release in a central synapse. *Nature* 450:676–682.
12. Zucker RS, Regehr WG (2002) Short-term synaptic plasticity. *Annu Rev Physiol* 64: 355–405.
13. Neher E, Sakaba T (2008) Multiple roles of calcium ions in the regulation of neurotransmitter release. *Neuron* 59:861–872.
14. Geppert M, et al. (1994) Synaptotagmin I: A major Ca2+ sensor for transmitter release at a central synapse. *Cell* 79:717–727.
15. DiAntonio A, Schwarz TL (1994) The effect on synaptic physiology of synaptotagmin mutations in Drosophila. *Neuron* 12:909–920.
16. Yoshihara M, Littleton JT (2002) Synaptotagmin I functions as a calcium sensor to synchronize neurotransmitter release. *Neuron* 36:897–908.
17. Nishiki T, Augustine GJ (2004) Synaptotagmin I synchronizes transmitter release in mouse hippocampal neurons. *J Neurosci* 24:6127–6132.
18. Pang ZP, et al. (2006) Synaptotagmin-2 is essential for survival and contributes to Ca2+ triggering of neurotransmitter release in central and neuromuscular synapses. *J Neurosci* 26:13493–13504.
19. Pang ZP, Sun J, Rizo J, Maximov A, Südhof TC (2006) Genetic analysis of synaptotagmin 2 in spontaneous and Ca2+-triggered neurotransmitter release. *EMBO J* 25:2039–2050.
20. Wen H, Brehm P (2005) Paired motor neuron-muscle recordings in zebrafish test the receptor blockade model for shaping synaptic current. *J Neurosci* 25:8104–8111.
21. Silver RA, Momiyama A, Cull-Candy SG (1998) Locus of frequency-dependent depression identified with multiple-probability fluctuation analysis at rat climbing fibre-Purkinje cell synapses. *J Physiol* 510:881–902.
22. Fox MA, Sanes JR (2007) Synaptotagmin I and II are present in distinct subsets of central synapses. *J Comp Neurol* 503:280–296.
23. Littleton JT, Stern M, Perin M, Bellen HJ (1994) Calcium dependence of neurotransmitter release and rate of spontaneous vesicle fusions are altered in Drosophila synaptotagmin mutants. *Proc Natl Acad Sci USA* 91:10888–10892.
24. Hui E, et al. (2005) Three distinct kinetic groupings of the synaptotagmin family: Candidate sensors for rapid and delayed exocytosis. *Proc Natl Acad Sci USA* 102: 5210–5214.
25. Sugita S, et al. (2001) Synaptotagmin VII as a plasma membrane Ca(2+) sensor in exocytosis. *Neuron* 30:459–473.
26. Craxton M, Goedert M (1999) Alternative splicing of synaptotagmins involving transmembrane exon skipping. *FEBS Lett* 460:417–422.
27. Wölfel M, Lou X, Schneggenburger R (2007) A mechanism intrinsic to the vesicle fusion machinery determines fast and slow transmitter release at a large CNS synapse. *J Neurosci* 27:3198–3210.
28. Dittman JS, Regehr WG (1998) Calcium dependence and recovery kinetics of presynaptic depression at the climbing fiber to Purkinje cell synapse. *J Neurosci* 18: 6147–6162.
29. Wang LY, Kaczmarek LK (1998) High-frequency firing helps replenish the readily releasable pool of synaptic vesicles. *Nature* 394:384–388.
30. Stevens CF, Wesseling JF (1998) Activity-dependent modulation of the rate at which synaptic vesicles become available to undergo exocytosis. *Neuron* 21:415–424.
31. Sakaba T, Neher E (2001) Calmodulin mediates rapid recruitment of fast-releasing synaptic vesicles at a calyx-type synapse. *Neuron* 32:1119–1131.
32. Wang P, Chicka MC, Bhalla A, Richards DA, Chapman ER (2005) Synaptotagmin VII is targeted to secretory organelles in PC12 cells, where it functions as a high-affinity calcium sensor. *Mol Cell Biol* 25:8693–8702.
33. Schonn JS, Maximov A, Lao Y, Südhof TC, Sørensen JB (2008) Synaptotagmin-1 and -7 are functionally overlapping Ca2+ sensors for exocytosis in adrenal chromaffin cells. *Proc Natl Acad Sci USA* 105:3998–4003.
34. Sugita S, Shin OH, Han W, Lao Y, Südhof TC (2002) Synaptotagmins form a hierarchy of exocytotic Ca(2+) sensors with distinct Ca(2+) affinities. *EMBO J* 21:270–280.
35. Li C, Davletov BA, Südhof TC (1995) Distinct Ca2+ and Sr2+ binding properties of synaptotagmins. Definition of candidate Ca2+ sensors for the fast and slow components of neurotransmitter release. *J Biol Chem* 270:24898–24902.
36. Gustavsson N, et al. (2009) Synaptotagmin-7 is a principal Ca2+ sensor for Ca2+-induced glucagon exocytosis in pancreas. *J Physiol* 587:1169–1178.
37. Fukuda M, Kanno E, Satoh M, Saegusa C, Yamamoto A (2004) Synaptotagmin VII is targeted to dense-core vesicles and regulates their Ca2+-dependent exocytosis in PC12 cells. *J Biol Chem* 279:52677–52684.
38. Li J, et al. (2009) Silence of Synaptotagmin VII inhibits release of dense core vesicles in PC12 cells. *Sci China C Life Sci* 52:1156–1163.
39. Maximov A, et al. (2008) Genetic analysis of synaptotagmin-7 function in synaptic vesicle exocytosis. *Proc Natl Acad Sci USA* 105:3986–3991.
40. Groffen AJ, et al. (2010) Doc2b is a high-affinity Ca2+ sensor for spontaneous neurotransmitter release. *Science* 327:1614–1618.
41. Widera G, et al. (2000) Increased DNA vaccine delivery and immunogenicity by electroporation in vivo. *J Immunol* 164:4635–4640.